PAPER

Investigation of magnetically driven passage of magnetic nanoparticles through eye tissues for magnetic drug targeting

IOP Publishing Nanotechnology

Nanotechnology **31** (2020) 495101 (12pp) https://doi.org/10.1088/1361-6528/abb0b4

Investigation of magnetically driven passage of magnetic nanoparticles through eye tissues for magnetic drug targeting

Diana Zahn[1], Katja Klein[1], Patricia Radon[2], Dmitry Berkov[3], Sergey Erokhin[3], Edgar Nagel[1,4], Michael Eichhorn[5], Frank Wiekhorst[2] and Silvio Dutz[1,6]

[1] Institut für Biomedizinische Technik und Informatik, Technische Universität Ilmenau, Germany
[2] Physikalisch-Technische Bundesanstalt, Berlin, Germany
[3] General Numerics Research Lab, Jena, Germany
[4] Ophthalmic Practice, Rudolstadt, Germany
[5] Institut für Anatomie, LSII, Universität Erlangen-Nürnberg, Erlangen, Germany
[6] Leibniz Institute of Photonic Technology, Jena, Germany

E-mail: silvio.dutz@tu-ilmenau.de

Received 28 April 2020, revised 20 July 2020
Accepted for publication 19 August 2020
Published 21 September 2020

Abstract

This paper elucidates the feasibility of magnetic drug targeting to the eye by using magnetic nanoparticles (MNPs) to which pharmaceutical drugs can be linked. Numerical simulations revealed that a magnetic field gradient of 20 T m^{-1} seems to be promising for dragging magnetic multicore nanoparticles of about 50 nm into the eye. Thus, a targeting magnet system made of superconducting magnets with a magnetic field gradient at the eye of about 20 T m^{-1} was simulated. For the proof-of-concept tissue experiments presented here the required magnetic field gradient of 20 T m^{-1} was realized by a permanent magnet array. MNPs with an optimized multicore structure were selected for this application by evaluating their stability against agglomeration of MNPs with different coatings in water for injections, physiological sodium chloride solution and biological media such as artificial tear fluid. From these investigations, starch turned out to be the most promising coating material because of its stability in saline fluids due to its steric stabilization mechanism. To evaluate the passage of MNPs through the sclera and cornea of the eye tissues of domestic pigs (*Sus scrofa domesticus*), a three-dimensionally printed setup consisting of two chambers (reservoir and target chamber) separated by the eye tissue was developed. With the permanent magnet array emulating the magnetic field gradient of the superconducting setup, experiments on magnetically driven transport of the MNPs from the reservoir chamber into the target chamber via the tissue were performed. The resulting concentration of MNPs in the target chamber was determined by means of quantitative magnetic particle spectroscopy. It was found that none of the tested particles passed the cornea, but starch-coated particles could pass the sclera at a rate of about 5 ng mm^{-2} within 24 h. These results open the door for future magnetic drug targeting to the eye.

Keywords: magnetic drug targeting, magnetic field gradient, magnetic nanoparticles, magnetic particle spectroscopy

(Some figures may appear in colour only in the online journal)

1. Introduction

Conventional strategies for applying drugs into the eye suffer from specific problems: application of eye drops to the surface of the eye results in low drug concentrations in the vitreous body and the retina and systemic therapy by infusion or pills is limited by the blood–retina barrier and leads to stronger adverse systemic effects. Intravitreal injection is currently the most effective procedure for applying drugs to the retina, but is associated with patient discomfort and serious risks such as endophthalmitis. Thus, a non-invasive and effective method for drug administration for common eye diseases such as age-related macular disease, diabetic retinopathy and retinal vein occlusion is very desirable.

An emerging strategy for overcoming the drawbacks of common drug application methods is the use of magnetic nanoparticles (MNPs) as targetable drug carriers. This method should minimize unwanted side effects caused by systemic drug administration, increase the drug concentration at the desired site of action and keep the drug in the target region for longer before it is cleared by physiological processes [1–3]. Nanoparticles used for delivering drugs can be targeted via several methods:

(I) Passive targeting uses the enhanced permeability and retention effect (EPR) as observed for different tumours. Thus, nanoparticles tend to accumulate in a tumour because of its increased vascularization [4, 5].
(II) For active targeting the nanoparticles are coupled to targeting ligands such as antibodies or aptamers, which are able to bind to unique receptors of the cells that are targeted [6–9].
(III) When MNPs are used as drug carriers, physical targeting strategies can direct the MNPs to the desired tissue by generating an attractive magnetic force acting on the MNPs via a magnetic field gradient [10–18].

In the case of magnetic targeting some challenges have still to be overcome, for example generating a field gradient large enough to move MNPs though viscous media or tissue, even at larger distances from the source of the magnetic field. Therefore, up to now magnetic targeting has often been investigated using *in vitro* models, where MNPs are moved inside vessel phantoms with the help of permanent magnets [19, 20], electromagnets [21, 22] or the field generated inside magnetic resonance imaging (MRI) [23] and magnetic particle imaging [24] scanners. In *in vivo* studies, administration via the circulatory system is the most common strategy, where MNP suspensions are injected intra-arterially or intravenously and directed to an organ or a part of the body with the help of a field gradient generated by magnets or MRI scanners [11, 14, 15, 18, 25].

Some attempts have been made to deliver MNPs through tissue instead of vessels. Gao *et al* investigated the passage of superparamagnetic iron oxide nanoparticles (SPIONs) through a three-layer cell phantom, modelling the round window membrane (RWM) of the human ear, using a permanent magnet [26]. A similar *in vivo* approach was adopted by Du *et al* in guinea pigs, where again SPIONs were directed through the RWM by the help of a permanent magnet placed on the opposite side of the head [27]. To overcome the decreasing magnetic field gradient with increasing distance between MNPs and the field gradient generating system, which is a problem for many applications at human scales, Shapiro and his group suggested a magnetic push instead of pull approach. Magnets can be arranged so that their fields create a point in front of the magnets where they cancel each other, thereby creating a gradient from the magnets to this point, leading to a pushing force on particles placed in this area [28]. This approach was used to push MNPs through the RWM in rats, but with the magnet setup placed at the working distance that would be needed in a human head [29]. The same approach was used in experiments in rats to push MNPs coated with starch and placed inside a contact lens into the eye [30]. The eye as a potential site for magnetic drug targeting was also investigated by Dengler *et al* [31]. After systemic administration of MNPs into the tail vein of mice, a permanent magnet was placed above their heads for 30 min, leading to the accumulation of a greater number of MNPs in eye tissue, as detected afterwards. However, the MNPs were found in all organs and the concentration of particles trapped in eye tissue was relatively low. Yanai *et al* administered stem cells labelled with MNPs systemically as well as by injection into the vitreous body of rats, and a small permanent magnet was placed inside the orbit behind the eye. This led to accumulation of stem cells in the retina at the site of the magnet (with both methods of administration), but intravitreal injection resulted in greater targeting efficiency [32].

To date no approach has been developed for injection-free, non-systemic delivery of drug-carrying MNPs into the human eye using a magnetic setup for pulling the particles into the eye.

When using a magnet system generating a time-invariant magnetic field gradient, the direction of the gradient is towards the magnet system and particles are attracted to the magnet system. Thus, the gradient-generating element has to be placed beside or behind the eye to obtain movement of the MNPs towards the inner eye. This requires a certain distance between the magnet and the eye. In a previous study [33] we designed a permanent magnet array for this purpose. Using permanent magnets, due to the relatively low remanence of NdFeB (maximum 1.5 T), the maximum possible field gradient at the eye was 5 T m^{-1} when the array was mounted beside/behind the eye. This field gradient was found to be far too low for effective transport of MNPs to the eye.

Therefore, in this study a superconducting magnet system was simulated which generates a magnetic field gradient of about 20 T m^{-1} at the eye even when the magnet is placed beside or behind the eye. For a proof-of-concept we used a permanent magnet array (emulating the simulated field gradient of the superconducting magnet system) to test if the 20 T m^{-1} gradient is strong enough for the MNPs to penetrate the tissue. To this end we developed a setup in which the permanent magnet can be placed very close to the eye tissues and will generate a field gradient of 20 T m^{-1} towards the inner eye. Further, we explored the possibility of preparing MNPs with

optimized properties for this purpose as well as strategies for the targeting process and technologies to evaluate and quantify the success of the targeting.

2. Methods

2.1. Synthesis of the MNPs

The magnetic multicore nanoparticles, which are interesting for many different medical applications [34], were prepared as described before [35, 36] by a method similar to the established wet co-precipitation method [37] but with a slower rate of addition of the alkaline medium and thereby a slower reaction velocity. In short, a $FeCl_2/FeCl_3$ solution (ratio of $Fe^{2+}/Fe^{3+} = 0.6$) was prepared with a total iron salt concentration of 0.6 M to which a 1.2 M $NaHCO_3$ solution was added continuously at a rate of 1.2 ml min^{-1} under permanent stirring. The thus formed non-magnetic precipitate was heated to 100 °C for 5 min to transfer it to a magnetic phase under the release of CO_2. The resulting magnetite/maghemite nanoparticles were washed three times with deionized water by magnetic separation to remove excess reaction products.

2.2. Coating of MNPs and preparation of ferrofluids

To obtain stable aqueous suspensions of MNPs (ferrofluids) and enhance their biocompatibility it is necessary to add a coating to the bare iron oxide particles. To investigate which coating is the most suitable for targeting to the eye several coating materials were tested, namely starch, carboxymethyldextran (CMD), dextran (DEX), citric acid (CA), polyethylenglycol (PEG) and trisodium citrate (NaZ). The coating procedure was similar for all the materials: 1 M HCl was added to the aqueous solution of bare MNPs until the pH reached 2−3 and ultrasonic treatment was applied to disintegrate potentially existing agglomerates and separate the single MNPs prior to the coating process. A solution of 10 wt% of the coating material in deionized water was added to the MNP suspension under stirring at 45 °C (50 °C for starch coating). The suspension was continuously stirred for 1 h, and in case of starch coating, ultrasonic treatment was applied every 10 min to prevent agglomeration. The coated particles were washed magnetically three times with deionized water to remove excess coating material and finally the particle concentration was adjusted to about 20 mg ml^{-1}.

2.3. Characterization of MNPs

The cluster size and size distribution of the multicore particles was investigated by means of transmission electron microscopy (TEM). For TEM from aqueous solutions of the MNPs, copper grids were rendered hydrophilic by argon plasma cleaning for 30 s. Ten microlitres of the respective sample solutions was applied to the grid, and excess sample was blotted with a filter paper. TEM images were acquired with a JEM-2010FEF (JEOL, Japan).

For determination of the hydrodynamic diameter of the coated MNPs, dynamic light scattering (DLS) was used (Zetasizer Nano ZS, Malvern Instruments, UK). Therefore, the sample was diluted 1:60 with deionized water and homogenized using an ultrasonic bath. The *z*-average of the intensity-weighted size distribution, derived from three consecutive measurements as the mean value, was used as a measure of the hydrodynamic particle size.

To analyse the surface charge of the coated MNPs, the zeta potential of the particles was measured with the same sample preparation scheme as for the hydrodynamic size measurements (Zetasizer Nano ZS). To measure the zeta potential, the viscosity and dielectric constant of the medium were taken as for water at 25 °C (0.8872 mPa*s and 78.5, respectively). All measurements were performed in three consecutive runs and obtained values were averaged.

The inner structure of the magnetic multicore nanoparticles was investigated by means of x-ray diffraction (XRD; Panalytical X'pert Pro, Malvern Panalytical, Almelo/The Netherlands). The results of the XRD investigations gave information about magnetic phase composition and the mean sizes of the primary cores which form the multicore particle. The size of the primary cores was calculated from measurements of the XRD line width using the Scherrer formula [38].

The magnetic characterization of all type of particles was done by vibrating sample magnetometry (VSM; Micromag 3900, Princeton Measurement Corporation, USA) at room temperature. From liquid samples and dry powders, the saturation magnetization (M_s), the coercivity (H_c), and the relative remanence (M_r/M_s) were determined. Taking into account the measured M_s of the plain magnetic cores, the particle concentration within the fluidic samples was calculated.

Table 1. Composition of the artificial tear fluid.

Chemicals	Concentration (mg/100 ml)
Sodium bicarbonate	192.4
Potassium chloride	111.0
Calcium chloride	2.3
Sodium chloride	672.8
Albumin	669.0
Glucose	2.5

2.4. Investigation of agglomeration stability of coated MNPs

To use MNPs for biological or medical applications it is necessary to ensure that they do not agglomerate in biological media. Turbidimetry via UV–Vis photometry (LLG-uniSPEC 2 Spectrophotometer, Lab Logistics Group GmbH, Germany) was used to investigate the stability of MNPs with different coatings in ultra-pure water for injection purposes (AMPUWA; Fresenius Kabi, Germany), physiological sodium chloride solution and artificial tears. The artificial tear fluid was prepared by dissolving the chemicals given in table 1 in deionized water [39].

As coating materials, starch, DEX, CMD, PEG, CA and NaZ were used for these experiments. All particle fluids were diluted to a MNP concentration of about

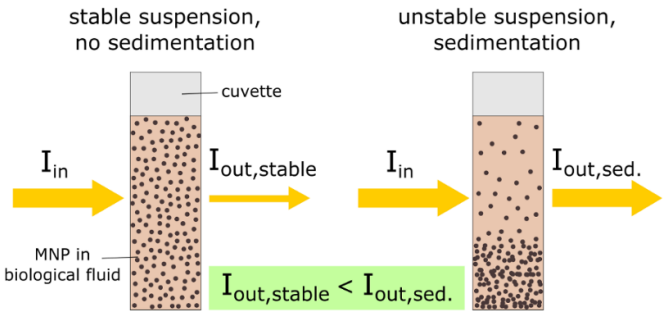

Figure 1. Principle used to investigate the stability of a MNP suspension by UV/Vis photometry (I is the light intensity).

0.35 mg ml^{-1} to obtain a concentration low enough to fulfil the pre-requirements of the Beer–Lambert law and to prevent the UV–Vis signal from reaching the saturation point. A total volume of 8 ml was prepared for each combination of MNP coating and biological fluid, which was then distributed to three cuvettes of 2 ml each. For each prepared sample of coated MNPs and biological fluid, absorption at a wavelength of 700 nm was measured for a period of 24 h. The three measurements were averaged, and the absorption values normalized to the initial value at $t = 0$. If the particles agglomerate the absorption value decreases because of a decrease in MNP concentration at the site of the absorption measurement in the upper portion of the cuvette due to sedimentation (see figure 1). In this study a particle system is declared as stable when the absorption value stays above 80% of the initial value for 24 h.

2.5. Simulation of superconducting targeting magnets

Simulation of the magnetic fields generated by a superconducting magnet is based on the standard assumption that superconducting currents in such a magnet flow along trajectories parallel to the side surfaces of the magnet (as sketched in the insets to figure 7 below). The volume of the magnet is discretized into cubical cells with sides of 1 mm, where superconducting current is considered constant in both amplitude and direction. Then the magnetic field distribution in the outside space is obtained from the Biot–Savart law. The current density of 1.13×10^9 A cm^{-2} is chosen in such a way that magnetic field distribution at the plane 2 mm above the square side of the 40 mm$\times$ 40 mm $\times$ 20 mm magnet corresponds to the experimental data from the magnet manufacturer. At this stage, the geometry of the cooling system surrounding the magnet is not considered but can easily be incorporated into our optimization methodology when required.

2.6. System for investigation of tissue passage

The passage of particles through eye tissue was evaluated with an experimental setup using 3D-printed chambers separated by *ex vivo* tissue samples from domestic pigs (*Sus scrofa domesticus*).

To prepare the eye tissue samples (figure 2), the remaining muscle tissue was removed from the pig eyes before they were

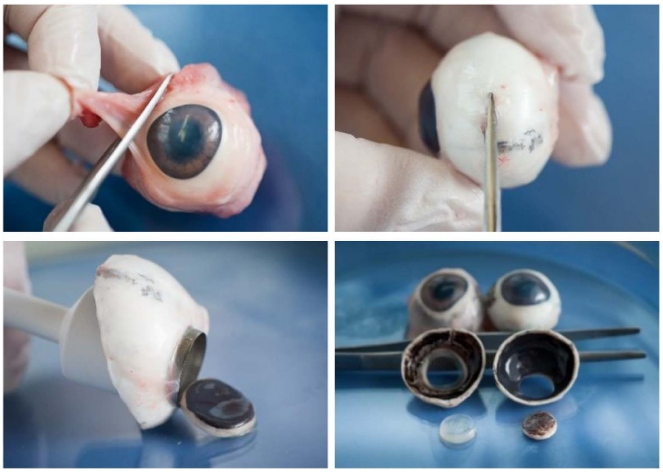

Figure 2. Preparation of eyes tissue samples from domestic pigs.

cut open. Then, the vitreous body, retina and choroid were removed, and disc-shaped samples of the sclera and cornea were extracted with a 12 mm biopsy punch. Samples were stored at −20 °C and thawed at room temperature before use. In preliminary studies no difference in tissue passage experiments was found between fresh tissue samples and thawed ones after storage at −20 °C.

The disposable chambers were printed with an SLA 3D Printer (ANYCUBIC Photon, ANYCUBIC, China). The reservoir chamber contained a suspension of MNPs (1.7 ml) and the target chamber (1.5 ml) deionized water, both chambers being separated by the tissue. The magnetically driven passage of particles through the tissue sample from one chamber to the other can be evaluated by applying a magnetic field gradient in the desired direction and examining whether particles pass the tissue and can be found in the target chamber. To realize a magnetic field gradient of about 20 T m^{-1} (resulting from simulations of the superconducting magnet, see section 3), a permanent magnet array, consisting of a row of four cubes with sides of 10 mm emulating the estimated field gradient of the superconducting magnet, was used. It was ensured that the permanent magnet array provided the desired gradient at the site of the tissue, 6 mm from the surface of the target chamber. The schematic setup of the complete system can be seen in figure 3.

2.7. Investigation of magnetically driven tissue passage

To investigate the passage of MNPs through eye tissue samples of cornea and sclera, the samples were placed between the two chambers and fixed by screwing the chambers together. The reservoir chamber was filled with 1.7 ml of the MNP suspension with a concentration of about 15–20 mg ml^{-1} and the target chamber contained 1.5 ml of deionized water. For the targeting experiments, MNPs coated with starch and DEX were used since they showed the most promising behaviour with regard to stability against agglomeration in biological media. CMD and CA were used in the targeting experiments as positive controls for unstable MNPs (see section 3). The

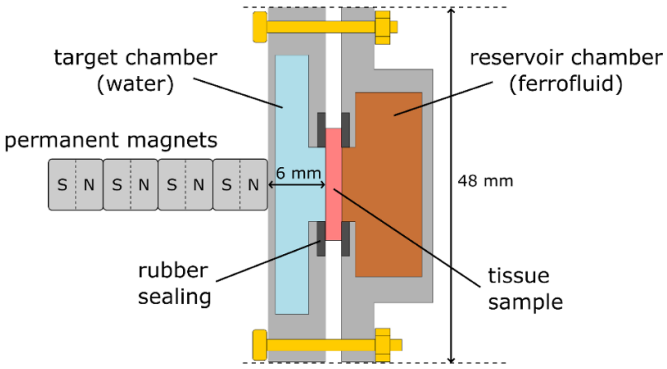

Figure 3. Schematic setup for evaluation of the tissue passage of MNPs.

permanent magnet was placed directly in front of the target chamber to allow the MNPs to penetrate and pass the tissue. After 24 h, the fluid in the target chamber was extracted and stored for further measurements. As a negative control, the same experiments were performed without applying a magnetic field gradient to investigate if the particles could penetrate the eye tissue even without a magnetic field gradient by means of particle diffusion.

The number of MNPs trapped in the target chamber was quantified by magnetic particle spectroscopy (MPS) using a commercial MPS device (MPS-3, Bruker, Germany). MPS detects the non-linear dynamic magnetization response of MNPs exposed to an oscillating excitation magnetic field. The third harmonic A_3 of the amplitude spectrum obtained by Fourier transformation of the MNP sample response is employed for quantification. $A_{3,\mathrm{smp}}$ is directly proportional to the amount of iron in the sample (smp). By comparison with the $A_{3,\mathrm{ref}}$ of a reference MNP sample (ref) with known amount of iron, $m_{\mathrm{Fe,ref}}$, the amont of iron in the MNPs, $m_{\mathrm{Fe,smp}}$, of a sample taken from the target chamber is determined as

$$m_{\mathrm{Fe,smp}} = m_{\mathrm{Fe,ref}} \frac{A_{3,\mathrm{smp}}}{A_{3,\mathrm{ref}}}$$

as described by Löwa *et al* [40]. Furthermore, to prove the validity of this relation we performed a serial dilution in water of the reference MNP system, varying the iron concentration of the sample. For all MPS measurements, an aliquot of 30 μl taken from the whole fluid was used. After quantifying the number of particles found in the target chamber, the number of permeated particles was normalized to the total tissue area that was exposed to the MNPs, to obtain a value in ng mm^{-2}.

3. Results and discussion

3.1. Structural and magnetic properties of the ferrofluids

Before using the prepared MNPs for investigating aggregation stability and drug targeting experiments, the structural and magnetic properties of the bare as well as the coated particles were investigated.

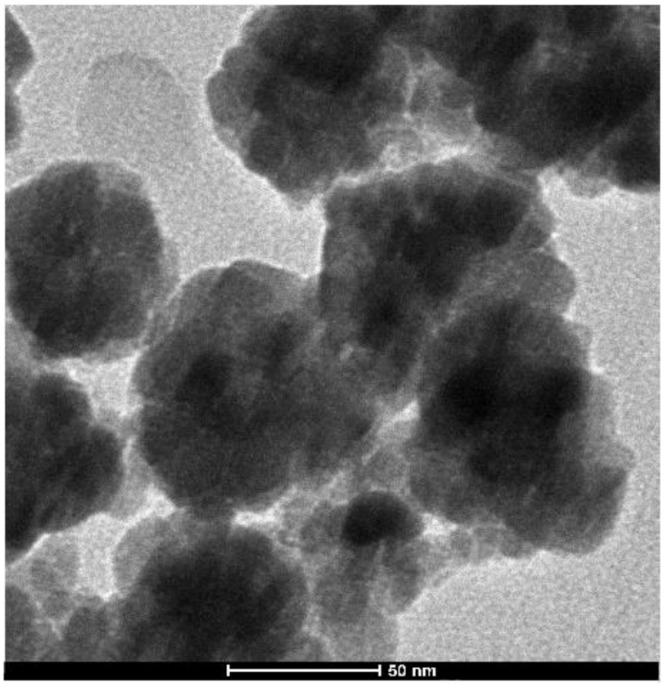

Figure 4. Typical TEM image of the prepared uncoated magnetic multicore nanoparticles.

The prepared bare particles had a mean diameter of 13.6 nm as determined by XRD. Phase identification by XRD (position of the 440 peak = 62.87°) demonstrated that the particles consist predominantly of maghemite with a small proportion of magnetite or solid solutions of both magnetic phases. For the bare particles, the mean hydrodynamic diameter obtained from DLS was 149 nm (polydispersity index = 0.12), indicating (in combination with the XRD results) a multicore particle structure with a relatively large cluster size. This was confirmed by TEM, where a mean cluster size of 45 ± 6.8 nm and a core size of 12−14 nm was found (see figure 4). A relatively narrow size distribution of cluster diameters was observed.

Dry powders of the bare MNPs show a ferromagnetic behaviour with a saturation magnetization (M_s) of 72.9 A m^2 kg^{-1}, a coercivity (H_c) of 1.59 kA m^{-1} and a relative remanence (M_r/M_s) of 0.04 (see figure 5).

Colloidal stable ferrofluids were prepared from the MNPs by coating the magnetic cores with different shell materials. The structural and magnetic properties of the obtained core/shell particles are summarized in table 2. Starch coating leads to large hydrodynamic diameters, since starch tends to aggregate during the coating process and build a matrix-like structure with MNPs embedded into it, rather than building up a coating layer around every single MNP. Due to this large amount of starch on the surface of the MNPs, their net magnetization is significantly lower than of the other particle systems used. In general, increasing hydrodynamic diameter is interpreted as agglomeration of MNPs before or during the coating process, rather than an increase in thickness of the coating. This is confirmed by magnetic measurements, where increasing hydrodynamic diameters are correlated with an increasing coercivity, which is caused by slower Brown

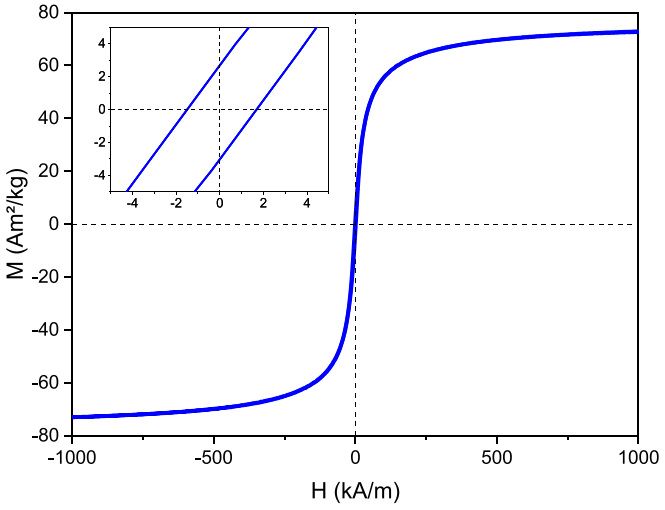

Figure 5. Magnetization curve of uncoated MNP powder. The inset depicts H_c and M_r.

relaxation due to a larger Brown diameter of strongly agglomerated particles. MNPs coated with CA and CMD do not show this trend, since CA is a very effective coating material which separates the single clusters within the soft agglomerates and CMD leads to very dense agglomerates with strong magnetic interactions between the single clusters [41].

From the obtained structural and magnetic properties, it can be concluded that the core/shell particles have a relatively large volume combined with a high saturation magnetization of the single particles but a low tendency to form agglomerates, which makes these particles promising for successful magnetic targeting.

3.2. Agglomeration stability of the core/shell MNPs

The stability of MNPs with different coatings in several biological media was investigated by means of turbidimetry. Measuring the absorption of a suspension in a UV–Vis photometer, one can observe a decreasing absorption value when particles are not stable, aggregated or agglomerated and finally sediment below the measurement window in the cuvette. Figure 6 shows the results of these measurements. In ultrapure water (AMPUWA) all coatings except NaZ show good stability over a 24 h period. The best agglomeration stability in sodium chloride solution or artificial tears was found for starch and DEX, due to their steric stabilization mechanism, which is more robust against the free ions present in saline media. For starch, the absorption stayed above the defined threshold of 0.8 for all three media, whereas the absorption for DEX falls below that in sodium chlorine solution (which serves as extreme benchmark) after 24 h. The fastest sedimentation was measured for PEG, CA, NaZ and CMD in NaCl, which can be seen in the rapid drop in the absorption values. However, in artificial tears, the particles (PEG, CA, NaZ) seem to be more stable, probably due to the proteins in the tear fluid which act like a stabilizer similar to tensides. In theory, PEG is expected to stabilize via a steric mechanism. This should lead to good stability in sodium chloride solution, contrary to the obtained results which might be due to a suboptimal coating, leaving some parts of the bare MNPs without a PEG layer. In conclusion, starch followed by DEX are the most promising coatings for application of the MNPs in biological systems and for medical purposes such as targeting to the eye.

3.3. Simulation of superconducting targeting magnets

Results of the calculation for the square (40 mm × 40 mm × 20 mm) and rectangular (120 mm × 40 mm × 20 mm) prismatic superconducting magnets are presented in figures 7 and 8. The magnetic field of the rectangular prismatic magnet is four times larger than that of the square prism, although the volume of the magnet in the first case is only three times larger. In both cases, the existence of only one current vortex in the magnet is assumed.

Preliminary computer optimization for a single square-prism superconducting magnet has shown that the average value of its magnetic field gradient (parallel to the desirable direction of the magnetic drag force) inside a vitreous body can reach ≈ 4 T m^{-1} and is thus comparable to the best values achieved by an optimized system of many Halbach arrays of NdFeB magnets [33]. Further studies employing two, three and four square prismatic superconducting magnets have shown an increase in the magnetic field gradient by 30%, 90% and 100%, respectively, in comparison with the single-magnet configuration.

As figure 8 shows, a rectangular-prism superconducting magnet not only provides a larger magnetic field than a square-prism system, but also a significantly more inhomogeneous magnetic field distribution; this inhomogeneity is a necessary prerequisite for a larger field gradient required to achieve a higher magnetic drag force $F \sim \nabla B$. Therefore, this non-square prism shape has been chosen for the superconducting magnet for the subsequent system optimization. We note that already a non-optimized placement (figure 8(b)) of such a magnet produces a relatively high value of the average field gradient (3.2 T m^{-1}) in the vitreous body.

The optimization procedure for superconducting magnet placement follows the method developed in [33], where magnetization orientations of magnetic moments for each magnet in a studied system were determined in order to maximize the average field gradient in the prescribed area. In the case of a single magnet, the following objective function is defined:

$$S = \Sigma_i S_i = \Sigma_i (\mathbf{n} \cdot \nabla B_i - \alpha_\perp (\mathbf{n}_\perp \cdot \nabla B_i)^2)$$

where i denotes a point inside the vitreous body (blue dots inside the eye in figure 8), $\mathbf{n}$ is the unit vector in the desirable direction of the magnetic drag force (blue arrows in the same figure), $\mathbf{n}_\perp$ is the unit vector in the picture plane perpendicular to $\mathbf{n}$ and ∇B_i is the magnetic field gradient. The first term in the sum favors the alignment of the magnetic field gradient along $\mathbf{n}$ and the second one is intended to avoid large perpendicular components of this gradient.

As the desired goal has been to optimize the placement of only one superconducting magnet, it is possible to calculate the objective function in the whole parameter space as

Table 2. Structural and magnetic properties of the obtained core/shell particles.

Coating material	z-average (nm)	Polydispersity index	Zeta potential (mV)	M_s (dry) (Am^2 kg^{-1})	H_c (fluid) (kA m^{-1})
Starch	296	0.18	−24	54.3	0.66
CMD	229	0.17	−32	66.6	1.82
CA	186	0.12	−32	69.8	0.17
DEX	178	0.15	16	65.1	0.58
PEG	133	0.10	25	66.1	0.54
NaZ	130	0.08	−44	70.1	0.50

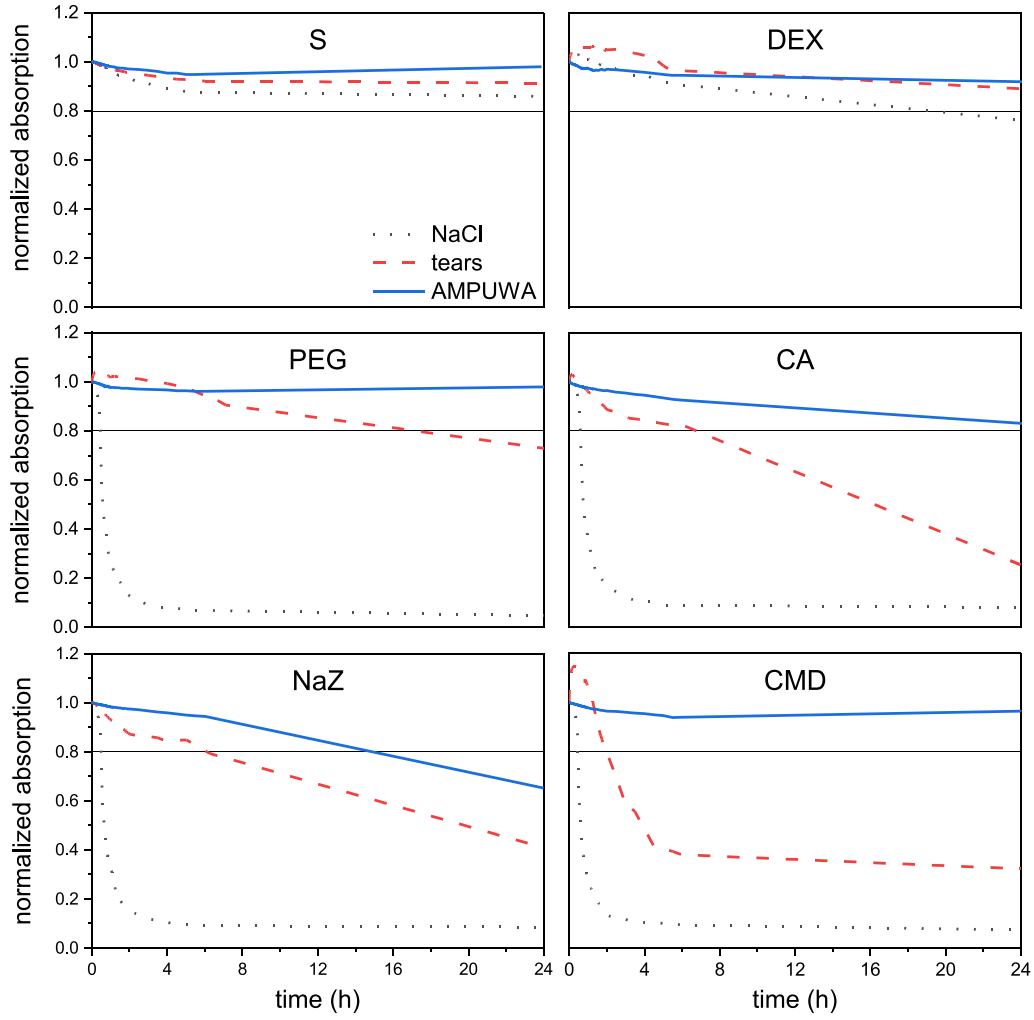

Figure 6. Turbidimetry measurements for investigation of the stability of particles with different coatings in sodium chloride solution (NaCl), simulated tears and AMPUWA. Absorption values after 24 h above 0.8 (black horizontal line) are defined as stable.

shown in figure 9. Position angle represents the placement of the magnet geometrical centre around the head (red dashed line in figure 8) and the rotation angle the orientation of the magnet with respect to its axis, which is perpendicular to the figure plane. The maximal value of the objective function corresponds to the rotational and angular positions of the rectangular-prism magnet depicted along with isolines of the generated magnetic field in figure 10(a).

The distribution of the absolute value of the magnetic field gradient and its directions in the vitreous body for the optimal case are shown in figure 10(b). For this configuration, the average component of the field gradient parallel to the desired magnetic force direction $S_{\|}$ is about 19 T m^{-1}. This value is almost four times larger than for the Halbach array of permanent NdFeB magnets studied in [33] and five times larger than for the single square-prism superconducting magnet.

3.4. System for investigation of tissue passage

The chamber setup was build using a stereolithographic 3D printer with UV-sensitive resin. The stereolithographic printing process, which builds up one layer after another from bottom to top in a reservoir of resin, enables the production of the hollow chambers in one piece. A rubber seal was mounted

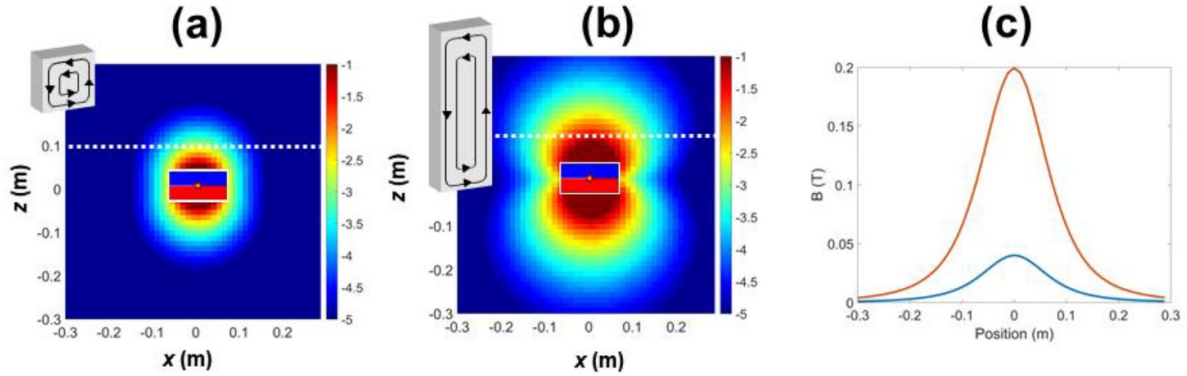

Figure 7. Comparison between calculated magnetic field distributions generated by superconducting magnets having the form of a square prism (a) and a rectangular prism (b) (logarithmic color scale, arbitrary units). (c) Magnetic field distribution along the white dotted lines shown in panels (a) and (b): blue solid line for the square prism (case (a)) and red solid line for the rectangular prism (case (b)).

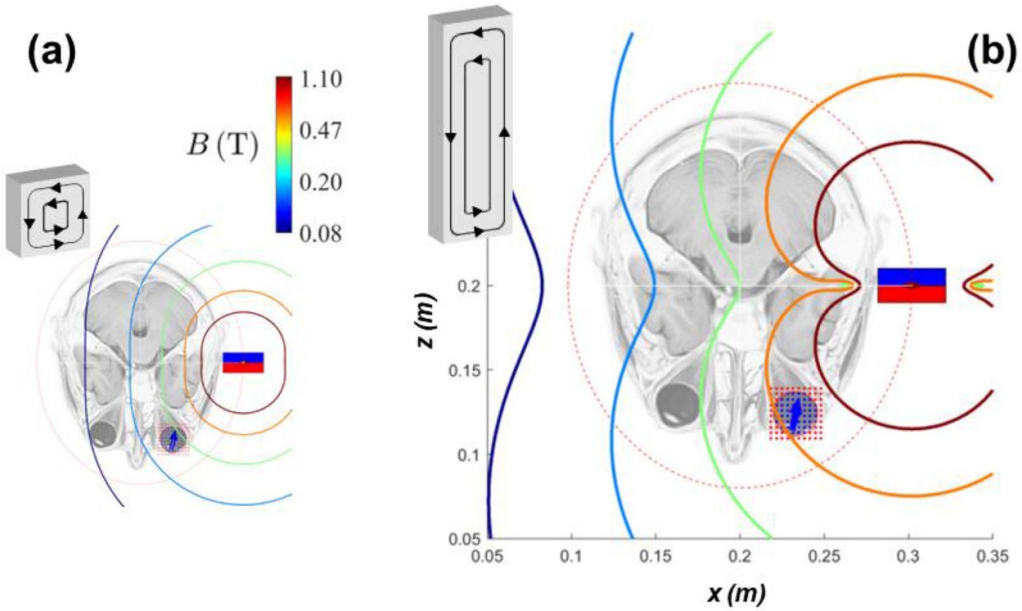

Figure 8. Isolines of the magnetic field magnitude B calculated for the square-prism (a) and rectangular-prism (b) superconducting magnets.

around the opening of the chambers to make sure that the tissue sample (see figure 3), which is used to separate the chambers, closes the window without leakages. The distance between the tissue sample and the rear wall of the target chamber is 6 mm. The magnetic system was placed on the surface of the rear wall of the target chamber, as shown in figure 11.

The permanent magnet array (four cubic NdFeB/N42 magnets with an edge length of 10 mm each, aligned in a row one dipole behind another) was characterized by means of a Gaussmeter (HGM09s, MAGSYS Magnet Systeme GmbH, Germany) to make sure that the emulated field gradient in the range of 20 T m^{-1} (see section 3) acts on the tissue sample. The obtained field mapping is shown in figure 12. At a distance of 6 mm from the surface, a field gradient between 23.5 T m^{-1} (in the centre of the magnet) and 18.6 T m^{-1} (4 mm from the centre in the x-direction, which corresponds to the radius of the targeting window of the chamber setup) was measured, leading to an averaged gradient at the whole cross section of the tissue sample above the window of about 21 T m^{-1}, which corresponds to the numerically estimated required field gradient.

3.5. Magnetically driven passage of MNPs through eye tissue

To investigate the passage of MNPs through tissue samples, MPS was used to quantify the number of MNPs in the target chamber. To check the range of validity of MPS quantification, we performed a serial dilution of the particle system (fluid as well as immobilized) and found a linear relationship of the moment A_3 with the amount of iron in the sample in the range of 3.6 ng to 189.3 μg. We therefore conclude MPS quantification for the MNPs over that range is valid without any significant particle–particle interaction at higher concentrations and a detection limit of 3.6 ng iron (see figure 13).

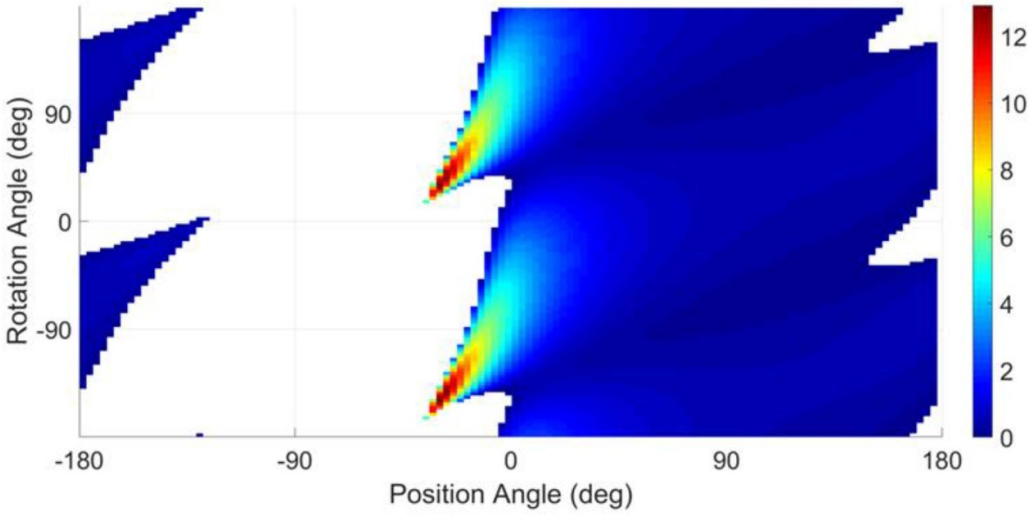

Figure 9. Dependence of the optimization function on rotation (around its own axis) and position (around head, see red dotted line in figure 10) angles of the rectangular-prism superconducting magnet. Negative values are ignored.

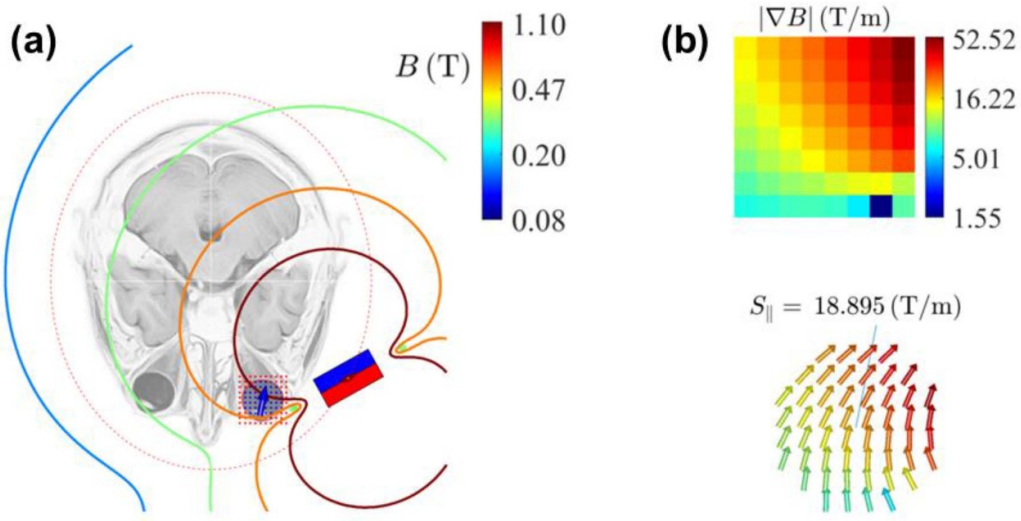

Figure 10. Optimized rotational and angular position of the rectangular-prism superconducting magnet. (a) Magnetic field distribution. (b) Magnetic field gradient distribution in a vitreous body of the human eye indicated by blue dots in panel (a). The blue arrow inside the eye shows the desirable direction of the magnetic drag force from the front surface of the eye to the retina.

There have been a few experiments where the tissue sample was decentred and did not ensure safe occlusion of the chambers, which could be seen after opening the chambers after 24 h. Those experiments were excluded from further data analysis.

Figure 14 shows the determined magnetic moment A_3 for all different coated samples taken from the targeting chamber for sclera tissue, with and without a magnetic field gradient. For all experiments with sclera samples without a magnet, no MNPs were detected in the target chamber. For experiments with sclera samples and an applied field gradient, significant passage of MNPs through the tissue was confirmed experimentally for starch-coated particles. In one experiment with CMD a very small number of MNPs were measured in the target chamber. Since the measured number of MNPs was very close to the detection limit, and thus is not reliable, this experiment was defined as no successful passage through the tissue. For DEX and CA, no MNPs were able to penetrate the sclera under the described conditions.

For experiments using cornea samples, no MNPs were found in the target chamber for any of the coatings used (starch, DEX, CA, CMD), neither with an applied magnetic gradient nor without (control experiment).

Considering the calibration curve for liquid samples from figure 13 and the determined magnetic moment in the targeting chamber as shown in figure 14, the total number of MNPs within the targeting chamber was calculated. This was then normalized to the area of the targeting window (meaning the tissue area exposed to the MNPs) of the chamber system, yielding the number of particles which penetrated an area of

Figure 11. Final setup consisting of 3D-printed chambers and the magnet array for targeting experiments.

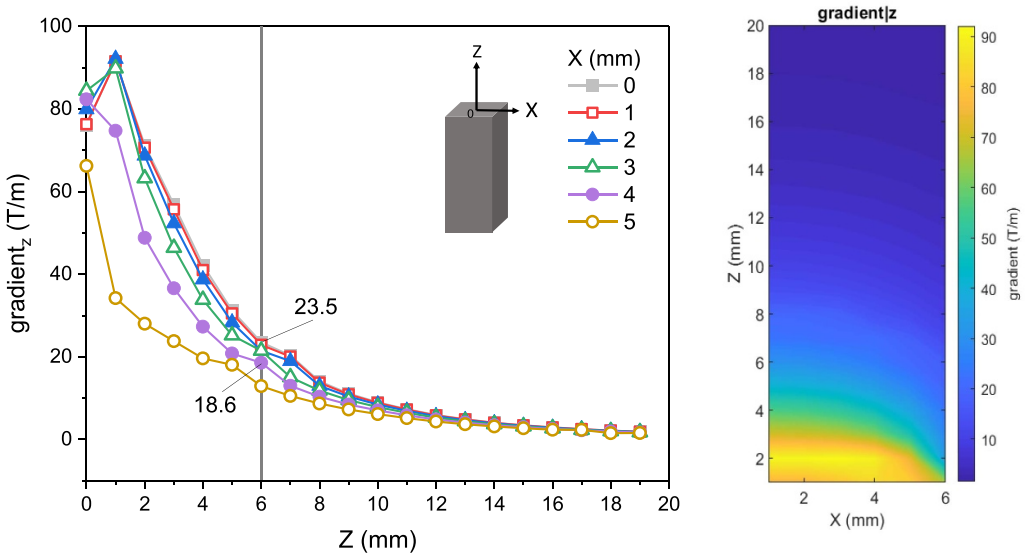

Figure 12. Magnetic field gradient in the z-direction of the permanent magnet in dependence on the distance Z to the surface and the distance X from the central axis of the magnet, shown as single curves (left) and field mapping (right). $X = 0$ mm represents the place in the centre of the tissue window and $X = 4$ mm the outer diameter (edge) of the tissue window.

tissue of 1 mm^2. The number of starch-coated particles that permeated the tissue was 5.4 ± 4.05 ng mm^{-2} (averaged over $n = 8$ experiments) after 24 h.

Although the results show a strong standard deviation, they confirm that magnetically driven transport of MNPs coated with starch through the sclera was successful. For each of the eight runs, a significant number of MNPs were detected in the targeting chamber. From our tested coating materials, starch turned out to be the most promising material for drug targeting into the eye. Since the starch-coated MNPs show a very thick coating with a relatively low resulting saturation magnetization (see table 2), the suitability of the starch coating for tissue penetration is not due to the effective magnetic moment of these particles but rather to the biochemical interaction between the starch surface and the tissue.

4. Conclusion

This work reports the first successful attempts to target magnetic multicore nanoparticles to the eye for drug targeting purposes. MNPs with optimized magnetic and structural properties were synthesized, showing high magnetization values ($M_s = 72.9$ Am^2 kg^{-1}), necessary for an efficient magnetic targeting, and low coercivity ($H_c = 1.59$ kA m^{-1}) and remanence at the same time, preventing them from agglomerating. As a coating material, starch turned out to be the most stable in biological fluids, (as determined by turbidimetry), preventing the particles from aggregating and sedimenting. Simulations were made to ensure the highest achievable field gradient generated by superconducting magnets in a human head at a working distance to the eye. This gradient, around 20 T m^{-1},

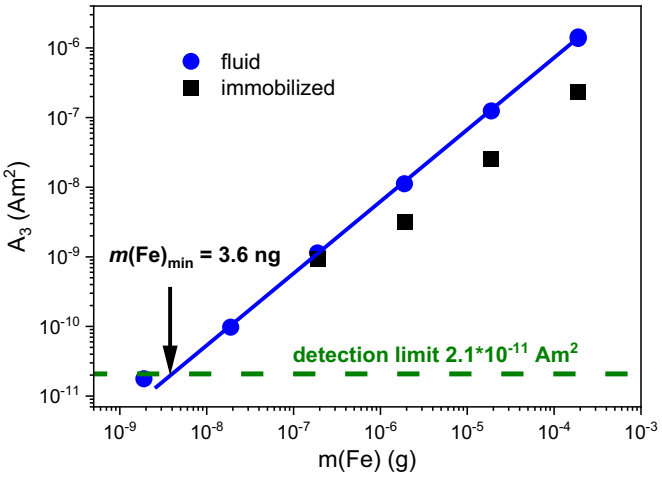

Figure 13. Calibration curve for the magnetic moment A_3 of fluid and immobilized MNPs in dependence on the iron content of the sample, measured by MPS.

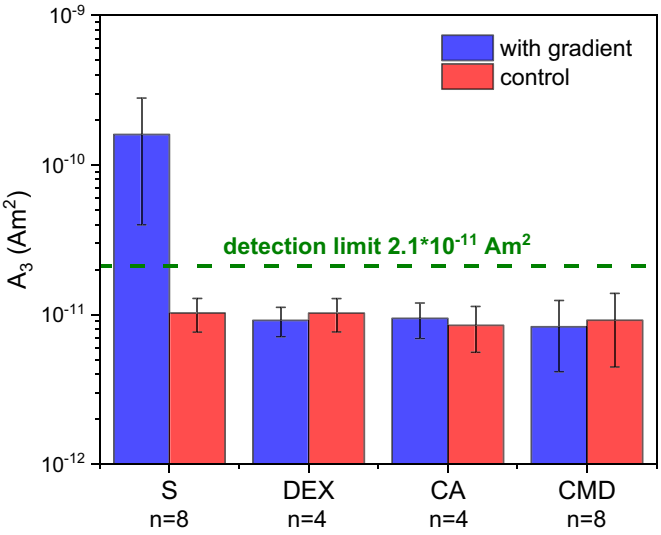

Figure 14. Magnetic moment A_3 of 30 μl samples from the targeting chamber for all different coatings tested with sclera tissue with or without an applied magnetic field gradient, measured by means of MPS.

was emulated by a simple setup of permanent magnets for the proof-of-concept *ex vivo* experiments presented here, in which the passage of MNPs through samples of sclera and cornea tissue was examined using a 3D-printed, disposable chamber setup. No particles could penetrate the cornea, whereas starch-coated particles were able to pass the sclera tissue driven by a magnetic gradient. Five nanograms of starch-coated MNPs per mm^2 of ferrofluid-exposed tissue was successfully transported magnetically through the tissue within 24 h. Although the number of penetrated MNPs is relatively low, our investigations show the feasibility of magnetic delivery of starch-coated MNPs, that could be used as drug carriers, into the eye. Our findings open the door for future magnetic drug targeting to the eye. In the next step, the simulated superconducting magnet system has to be built and used for a targeting study, similar to the work described in this study.

Acknowledgments

This work is supported by the Freistaat Thüringen (contract 2016 FE 9100) and is co-financed by the European Union in the frame of the 'European Regional Development Fund (ERDF)'. Funding was provided by the DFG core facility, grant numbers KO5321/3 and TR408/11 for the MPS quantification measurements. The authors thank Dr Minzhi Wu (Magnetworld AG, Jena, Germany) for providing the permanent magnets for the targeting experiments and Mühlhäuser Fleisch GmbH (Mühlhausen, Germany) for providing the animal tissue samples.

ORCID iDs

Diana Zahn https://orcid.org/0000-0001-7478-4256
Katja Klein https://orcid.org/0000-0003-3022-6265
Patricia Radon https://orcid.org/0000-0002-4032-5067
Dmitry Berkov https://orcid.org/0000-0003-3883-5161
Sergey Erokhin https://orcid.org/0000-0001-8449-3612
Edgar Nagel https://orcid.org/0000-0002-6179-0160
Michael Eichhorn https://orcid.org/0000-0001-9005-3322
Frank Wiekhorst https://orcid.org/0000-0003-0608-1473
Silvio Dutz https://orcid.org/0000-0002-7258-0943

References

[1] Arruebo M, Fernández-Pacheco R, Ibarra M R and Santamaría J 2007 Magnetic nanoparticles for drug delivery *Nano Today* **2** 22–32
[2] Dunuweera S P, Rajapakse R M S I, Rajapakshe R B S D, Wijekoon S H D P, Nirodha Thilakarathna M G G S and Rajapakse R M G 2019 Review on targeted drug delivery carriers used in nanobiomedical applications *Curr. Nanosci.* **15** 382–97
[3] El-Boubbou K 2018 Magnetic iron oxide nanoparticles as drug carriers: preparation, conjugation and delivery *Nanomedicine* **13** 929–52
[4] Blanco E, Shen H and Ferrari M 2015 Principles of nanoparticle design for overcoming biological barriers to drug delivery *Nat. Biotechnol.* **33** 941–51
[5] Shi J, Kantoff P W, Wooster R and Farokhzad O C 2017 Cancer nanomedicine: progress, challenges and opportunities *Nat. Rev. Cancer* **17** 20–37
[6] Bertrand N, Wu J, Xu X, Kamaly N and Farokhzad O C 2014 Cancer nanotechnology: the impact of passive and active targeting in the era of modern cancer biology *Adv. Drug Delivery Rev.* **66** 2–25
[7] Heath T D, Fraley R T and Papahdjopoulos D 1980 Antibody targeting of liposomes: cell specificity obtained by conjugation of F(ab′)2 to vesicle surface *Science* **210** 539
[8] Hrkach J *et al* 2012 Preclinical development and clinical translation of a PSMA-targeted docetaxel nanoparticle with a differentiated pharmacological profile *Sci. Transl. Med.* **4** 128ra39
[9] Wang X Q, Li R F, Zhu Y X, Wang Z C, Zhang H R, Cui L Q, Duan S F and Guo Y Q 2020 Active targeting co-delivery of therapeutic Sur siRNA and an antineoplastic drug via epidermal growth factor receptor-mediated magnetic

nanoparticles for synergistic programmed cell death in glioblastoma stem cells *Mater. Chem. Front.* **4** 574–88
[10] Banis G, Tyrovolas K, Angelopoulos S, Ferraro A and Hristoforou E 2020 Pushing of magnetic microdroplet using electromagnetic actuation system *Nanomaterials* **10** 371
[11] Chertok B, David A E and Yang V C 2010 Polyethyleneimine-modified iron oxide nanoparticles for brain tumor drug delivery using magnetic targeting and intra-carotid administration *Biomaterials* **31** 6317–24
[12] Johnson C D L *et al* 2019 Injectable, magnetically orienting electrospun fiber conduits for neuron guidance *ACS Appl. Mater. Interfaces* **11** 356–72
[13] Marcus M, Smith A, Maswadeh A, Shemesh Z, Zak I, Motiei M, Schori H, Margel S, Sharoni A and Shefi O 2018 Magnetic targeting of growth factors using iron oxide nanoparticles *Nanomaterials* 8
[14] Matuszak J, Lutz B, Sekita A, Zaloga J, Alexiou C, Lyer S and Cicha I 2018 Drug delivery to atherosclerotic plaques using superparamagnetic iron oxide nanoparticles *Int. J. Nanomed.* **13** 8443–60
[15] Mojica Pisciotti M L *et al* 2014 In vitro and in vivo experiments with iron oxide nanoparticles functionalized with DEXTRAN or polyethylene glycol for medical applications: magnetic targeting *J. Biomed. Mater. Res.* B **102** 860–8
[16] Muthana M *et al* 2015 Directing cell therapy to anatomic target sites *in vivo* with magnetic resonance targeting *Nat. Commun.* **6** 8009
[17] Nishida K, Tanaka N, Nakanishi K, Kamei N, Hamasaki T, Yanada S, Mochizuki Y and Ochi M 2006 Magnetic targeting of bone marrow stromal cells into spinal cord: through cerebrospinal fluid *NeuroReport* **17** 1269–72
[18] Tietze R *et al* 2013 Efficient drug-delivery using magnetic nanoparticles - biodistribution and therapeutic effects in tumour bearing rabbits *Nanomed. Nanotechnol. Biol. Med.* **9** 961–71
[19] Pernal S P, Willis A J, Sabo M E, Moore L M, Olson S T, Morris S C, Creighton F M and Engelhard H H 2020 An *in vitro* model system for evaluating remote magnetic nanoparticle movement and fibrinolysis *Int. J. Nanomed.* **15** 1549–68
[20] Radon P, Löwa N, Gutkelch D and Wiekhorst F 2016 Design and characterization of a device to quantify the magnetic drug targeting efficiency of magnetic nanoparticles in a tube flow phantom by magnetic particle spectroscopy *J. Magn. Magn. Mater.* **427** 175–80
[21] Do T D, Noh Y, Kim M O and Yoon J and 2015 An electromagnetic steering system for magnetic nanoparticle drug delivery *12th Int. Conf. on Ubiquitous Robots and Ambient Intelligence* (New York: IEEE) 528–31
[22] Tehrani M D, Kim M O and Yoon J 2014 A novel electromagnetic actuation system for magnetic nanoparticle guidance in blood vessels *IEEE Trans. Magn.* **50** 1–12
[23] Li N *et al* 2019 Magnetic resonance navigation for targeted embolization in a two-level bifurcation phantom *Ann. Biomed. Eng.* **47** 2402–15
[24] Griese F, Knopp T, Gruettner C, Thieben F, Muller K, Loges S, Ludewig P and Gdaniec N 2020 Simultaneous magnetic particle imaging and navigation of large superparamagnetic nanoparticles in bifurcation flow experiments *J. Magn. Magn. Mater.* **498** 12
[25] Pouponneau P, Leroux J C, Soulez G, Gaboury L and Martel S 2011 Co-encapsulation of magnetic nanoparticles and doxorubicin into biodegradable microcarriers for deep tissue targeting by vascular MRI navigation *Biomaterials* **32** 3481–6
[26] Gao X, Wang Y, Chen K, Grady B, Dormer K and Kopke R 2010 Magnetic assisted transport of PLGA nanoparticles through a human round window membrane model *J. Nanotechnol. Eng. Med.* **1** 031010
[27] Du X, Chen K, Kuriyavar S, Kopke R D, Grady B P, Bourne D H, Li W and Dormer K J 2013 Magnetic targeted delivery of dexamethasone acetate across the round window membrane in guinea pigs *Otol. Neurotol.* **34** 41–47
[28] Shapiro B, Dormer K and Rutel I B 2010 A two-magnet system to push therapeutic nanoparticles *AIP Conf. Proc.* **1311** 77–88
[29] Sarwar A, Lee R, Depireux D and Shapiro B 2013 Magnetic injection of nanoparticles into rat inner ears at a human head working distance *IEEE Trans. Magn.* **49** 440–52
[30] Shapiro B, Kulkarni S, Nacev A, Sarwar A, Preciado D and Depireux D A 2014 Shaping magnetic fields to direct therapy to ears and eyes *Annu. Rev. Biomed. Eng.* **16** 455–81
[31] Dengler M, Saatchi K, Dailey J P, Matsubara J, Mikelberg F S, Häfeli U O and Yeung S N 2010 Targeted delivery of magnetic cobalt nanoparticles to the eye following systemic administration *AIP Conf. Proc.* **1311** 329–36
[32] Yanai A, Hafeli U O, Metcalfe A L, Soema P, Addo L, Gregory-Evans C Y, Po K, Shan X, Moritz O L and Gregory-Evans K 2012 Focused magnetic stem cell targeting to the retina using superparamagnetic iron oxide nanoparticles *Cell Transplant.* **21** 1137–48
[33] Erokhin S and Berkov D 2019 Magnetic targeted drug delivery to the human eye retina: an optimization methodology *IEEE J. Electromagn. RF Microw. Med. Biol.* **3** 3–8
[34] Dutz S 2016 Are magnetic multicore nanoparticles promising candidates for biomedical applications? *IEEE Trans. Magn.* **52** 0200103
[35] Dutz S, Andrae W, Hergt R, Mueller R, Oestreich C, Schmidt C, Toepfer J, Zeisberger M and Bellemann M E 2007 Influence of dextran coating on the magnetic behaviour of iron oxide nanoparticles *J. Magn. Magn. Mater.* **311** 51–54
[36] Dutz S, Clement J H, Eberbeck D, Gelbrich T, Hergt R, Mueller R, Wotschadlo J and Zeisberger M 2009 Ferrofluids of magnetic multicore nanoparticles for biomedical applications *J. Magn. Magn. Mater.* **321** 1501–4
[37] Khalafalla S E and Reimers G W 1980 Preparation of dilution-stable aqueous magnetic fluids *IEEE Trans. Magn.* **16** 178–83
[38] Scherrer P 1918 *Nachrichten von der Gesellschaft der Wissenschaften zu Göttingen, Mathematisch-Physikalische Klasse* (Berlin: Weidmannsche Buchhandlung) pp 98–100
[39] Hagigit T, Nassar T, Behar-Cohen F, Lambert G and Benita S 2008 The influence of cationic lipid type on *in-vitro* release kinetic profiles of antisense oligonucleotide from cationic nanoemulsions *Eur. J. Pharm. Biopharm.* **70** 248–59
[40] Lowa N, Wiekhorst F, Metzkow S, Ludwig A and Trahms L 2013 Magnetic particle spectroscopy for the quantification of magnetic nanoparticles in living cells *Biomed. Eng.* **58** 2
[41] Dutz S and Hergt R 2012 The role of interactions in systems of single domain ferrimagnetic iron oxide nanoparticles *J. Nano-Electron. Phys.* **4** 20101–7